ELSEVIER

Biochimica et Biophysica Acta 1509 (2000) 131–147

BIOCHIMICA ET BIOPHYSICA ACTA
BBA

www.elsevier.com/locate/bba

Supported planar bilayer formation by vesicle fusion: the interaction of phospholipid vesicles with surfaces and the effect of gramicidin on bilayer properties using atomic force microscopy

Z.V. Leonenko, A. Carnini, D.T. Cramb *

Department of Chemistry, University of Calgary, 2500 University Dr. N.W., Calgary, Alta., Canada T2N 1N4

Received 28 February 2000; received in revised form 27 June 2000; accepted 7 July 2000

Abstract

We have used magnetic alternating current mode atomic force microscopy (MAC–AFM) to investigate the formation of supported phospholipid bilayers (SPB) by the method of vesicle fusion. The systems studied were dioleoylphosphatidylcholine (DOPC) on mica and mica modified with 3-aminopropyl-triethoxy-silane (APTES), and DOPC vesicles with gramicidin incorporated on mica and APTES-modified mica. The AFM images reveal three stages of bilayer formation: localized disklike features that are single bilayer footprints of the vesicles, partial continuous coverage, and finally complete bilayer formation. The mechanism of supported phospholipid bilayers formation is the fusion of proximal vesicles, rather than surface disk migration. This mechanism does not appear to be affected by incorporation of gramicidin or by surface modification. Once formed, the bilayer develops circular defects one bilayer deep. These defects grow in size and number until a dynamic equilibrium is reached.

Keywords: Dioleoylphosphatidylcholine; Elasticity; Fusion; Size distribution; Bilayer

1. Introduction

Investigations using supported phospholipid bilayers have been very successful in helping elucidate the physical behavior of cell membranes and the physical behavior of membrane-bound macromolecules. Supported planar bilayers (SPBs) are composed of phospholipids adsorbed to a planar hydrophilic solid support. SPBs have been used as model membranes to study cell–cell recognition in the immune system [1], adhesion of cells [2], phospholipid diffusion [3], protein binding to lipid ligands [4,5], membrane insertion of proteins [6], surface binding kinetics [7] and phospholipase A_2-induced bilayer hydrolysis [8]. The bulk of these studies have employed the Langmuir–Blodgett technique to prepare the bilayer. Bilayer properties are then examined using a variety of techniques including, but not limited to electrochemistry [9,10], fluorescence microscopy [11–13] and more recently atomic force microscopy (AFM) [14–17]. In order to be comparable with natural membranes, supported bilayers are often multicomponent and may include integral membrane proteins. Such systems can not be easily created by means of the Langmuir–Blodgett technique. This motivated attempts to develop a more protein-friendly method of supported bilayer production. The most successful is that of vesicle fusion, first

* Corresponding author. Fax: +1-403-289-9488;
E-mail: dcramb@ucalgary.ca

0005-2736/00/$ – see front matter
PII: S0005-2736(00)00288-1

described by Brian and McConnell [18]. This method involves the spreading of lipid vesicles from solution onto a surface [11,12].

Although the use of vesicle fusion is becoming more common in the preparation of supported bilayers, the process itself has yet to be observed at the molecular level. The two benchmark studies of SPB formation via vesicle fusion employ total internal reflectance microscopy using fluorescence recovery after photobleaching (TIR–FRAP) [12] and fluorescence quenching [13]. A common theme that emerged from these studies was that there are at least two stages in SPB formation. The first stage involves the deposition of vesicles which appear to be immobile once bound to the support. With increasing deposition time, the first stage turns over to a continuously covered surface where the phospholipids attain extended mobility. More recently, the kinetics of vesicle fusion have been investigated using interference contrast microscopy [19,20], quartz crystal microbalance [21] and ellipsometry [22]. An investigation of SPB formation via vesicle fusion at the nm length scale should shed light both on SPB formation and perhaps on any anomalous diffusion behavior observed in SPBs. Moreover, liposome–surface interactions are of inherent importance because over the last two decades liposomes have been increasingly used as a delivery vehicle for genetic material and hydrophobic pharmaceuticals [23].

The historic impediment to direct visualization of single soft macromolecules at the nm scale has been that its fluid nature precluded the use of electron, neutron and X-ray scattering techniques, except to obtain average heavy particle distances and angles. To overcome this, soft matter samples were examined using freeze–fracture techniques to lock in their structure and reduce random motion. AFM was developed to be an effective tool used to measure surface topography of reasonably inflexible materials at the nanometer scale. However, with the advent of the more gently 'tapping' mode used in AFM, it has become possible to image the topography of soft fluid-like matter. In fact, AFM has been employed to characterize the structure and stability of supported bilayers of dilinoleoylphosphatidylethanolamine in the liquid phase [15] and even to image the surface of living cells [24,25]. Very recently, Reviakine and Brisson [26] reported a study of the formation of supported bilayers by vesicle fusion on mica and SiO_2 using contact mode AFM. In their work, they observed a dependence of the fusion mechanism on vesicle size and method of preparation. Their results compared very favorably with the theoretical models of Siefert and Lipowsky [27,28]. Additionally, Pignataro et al. [29] examined biotin-mediated vesicle adhesion using AFM and quartz crystal microbalance.

In this work, using magnetic alternating current mode (MAC)–AFM we examined the process of SPB preparation on mica via vesicle fusion. Three distinct stages of bilayer growth are observed. The first consists of disk-like surface features associated with single vesicle deposition. In the second stage, there are areas of complete bilayer formation and areas with disks. In the last stage, a complete bilayer is formed. Interestingly, this bilayer develops defects that are found to be quite dynamic in nature. We have also examined the effect of mica surface modification and vesicular incorporation of the ion channel gramicidin on SPB formation via vesicle fusion.

2. Materials and methods

2.1. Sample preparation

Dioleoylphosphatidylcholine (DOPC) 20 mg/ml in chloroform (Sigma, Ont., Canada) was used without further purification. Purified gramicidin-AC2, HCO-L-Val-Gly-L-Ala-D-Leu-L-Ala-D-Val-D-Val-D-Val-L-Trp-D-Leu-L-Trp-D-Leu-L-Trp-D-Leu-L-Trp-$CONHCH_2CH_2OCONH(CH_2)_2NH_3^+$ (gram-AC2) was a generous gift of Professor G.A. Woolley (University of Toronto). It has been demonstrated [30] that gram-AC2 is more easily incorporated into DOPC vesicles than gramicidin A. The structures of DOPC and gram-AC2 are presented in Fig. 1. Acetate buffer, 0.01 M, pH 6.5 was freshly prepared and used in the generation of all vesicles. Distilled, ultrapure (Nanopure) water was used throughout this study. Chemically modified mica [31,32] was obtained by deposition of 10 μl of 0.01% aqueous solution of 3-aminopropyl-triethoxy-silane (APTES, Sigma, Ont., USA) onto freshly cleaved mica. After 5 min, the mica was rinsed with ultrapure water and dried with nitrogen. Mica has a layered structure, which

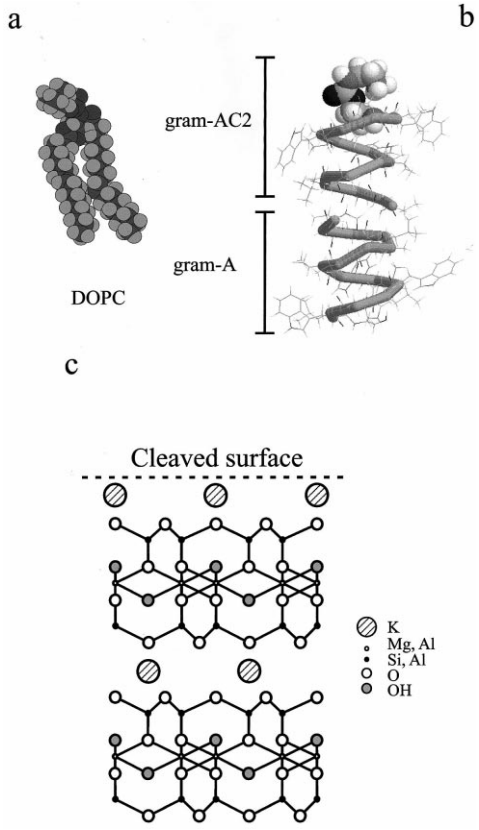

Fig. 1. (a) The structures of DOPC. (b) Gramicidin A and gramicidin-AC2. (c) The structure of a vertical slice through freshly cleaved muscovite mica.

reveals an atomically flat surface after cleavage. Mica consists of negatively charged layers that are bound together by large, positively charged interlayer cations, K^+ in the case of muscovite mica. Each stratum consists of two hexagonal layers of SiO_4, which are crosslinked by aluminum atoms with incorporated OH^- groups (see Fig. 1c). The electrostatic bonds between K^+ ions and O atoms from the layer are weak and easily broken. This layer is disrupted after a cleavage procedure, exposing a basal plane covered by K^+ ions, with the density 0.57 ions/nm [2,33]. When we modify mica with APTES, the amino groups give the surface a net positive charge. Moreover, it has been shown that an APTES-treated mica surface is more polar than pure mica [34].

All vesicles were prepared using the 'dry' method. That is, an appropriate aliquot of DOPC chloroform solution was measured into a small vessel and the chloroform removed using a stream of dry nitrogen. The dry DOPC was then suspended in buffer to its final concentration (e.g. 2.0 mg/ml), and stirred for 30 min. At this point, the solution was still quite cloudy due to the presence of large multilamellar vesicles. The solution was therefore sonicated (Branson 1200, Dansbury, CT, USA) for 10 min periods to obtain a more uniform distribution of vesicles in solution. Between each 10 min period, there was a 15 min 'rest' interval where the solution was cooled and stirred at room temperature. For this method, the solutions were cycled for an average of 10 times or until they were observed to clear. Gramicidin-AC2 (Gramicidin/DOPC mol fraction of 1/100) was incorporated into the vesicles by including an aliquot of the protein, dissolved in methanol, in the small vessel which contained dry DOPC. The methanol was then removed using dry nitrogen gas and the mixture was resuspended and sonicated as above.

2.2. AFM

AFM is a surface imaging technique with nm scale lateral resolution and 0.1 Å normal resolution, which operates by measuring the forces acting between a probe and a sample. We employed the MAC mode, where the magnetically coated probe oscillates near its resonant frequency driven by an alternating magnetic field. For the MAC mode, changes in height and phase shift (friction) are measured during the scan [35,36]. This technique has proven to be advantageous for measuring soft samples in liquid media. All images were taken using a Pico SPM microscope with AFMS-165 scanner (Molecular Imaging Inc., Phoenix, AZ, USA). Au–Cr coated Maclevers (Molecular Imaging Inc.) were used for MAC mode imaging. Their specifications are; length: 85 μm, force constant: 0.5 N/m and resonant frequency 38 kHz in liquid. The standard MAC mode fluid cell (Molecular Imaging) was used throughout. The scanning speed was 7–9 lines per second for areas of a few hundred nm per side and 2–3 lines per second for the areas of a few μm per side.

Samples were prepared for AFM imaging in the following way. Aliquots of 20 μl liposome solution were deposited on modified or unmodified freshly cleaved ASTMV-2 quality, scratch-free ruby mica (Asheville–Schoonmaker Mica Co., VA, USA). After a controlled period of time the mica was gently rinsed with ultrapure water. The sample chamber

was then mounted onto the AFM scanner. All samples were imaged in ultrapure water because we have observed degradation in image quality with increasing ionic strength. Indeed, the highest contrast images were always obtained by imaging in ultrapure water. In an attempt to minimize the osmotic shock to vesicles during rinsing, the original solutions were thus prepared with a low ionic strength. This rinsing process occurs before the AFM tip encounters the solution. Therefore, the tip is never exposed to a liposome solution. All liposome solutions were sonicated for an additional 15–20 min and then allowed to return to room temperature before imaging.

2.3. Dynamic light scattering (DLS)

DLS experiments were performed using a Brookhaven instrument (Brookhaven, CT, USA) on the vesicle preparations at a scattering angle of 90°. The light scattering data were analyzed following the method of cumulants [37] to obtain the hydrodynamic radii of the vesicles.

3. Results

After solutions containing sonicated phospholipids at densities of 0.1–7.0 mg/ml either with or without gram-AC2 in acetate buffer were brought into contact with freshly cleaved mica surfaces or modified freshly cleaved mica surfaces, MAC–AFM images were then collected in an ultrapure water environment to achieve the highest resolution. Analysis of the resulting images suggested three regimes for vesicle fusion: the early stage, where only disklike features are apparent; the intermediate stage where fusion begins and there is a combination of continuously covered areas and areas with disklike features; and the final stage, where surface coverage is complete and is presumably a bilayer of phospholipids. We summarize the various stages of vesicle fusion for the combinations of surface modification and protein incorporation in Tables 1 and 2.

Table 1
DOPC vesicles adsorption on modified and unmodified mica using MAC–AFM

Concentration and time of adsorption (mg/ml, min)	Result on modified mica	Result on unmodified mica
0.1, 1	vesicles	no vesicles
0.2, 1	vesicles+layer	no vesicles
0.2, 2	layer	no vesicles
0.2, 3	layer	no vesicles
0.2, 5	layer	vesicles

Table 2
DOPC–gram-AC vesicles adsorption on modified and unmodified mica using MAC–AFM

Concentration and time of adsorption (mg/ml, min)	Result on modified mica	Result on unmodified mica
0.1, 1	no vesicles	no vesicles
0.2, 1	no vesicles	no vesicles
0.2, 2	vesicles	no vesicles
0.5, 2	layer	no vesicles
0.7, 2	layer	no vesicles
4.7, 2	layer	vesicles
7, 2	layer	layer

3.1. Early stage: liposome adsorption

A typical image of APTES-modified mica exposed to a 0.1 mg/ml solution of DOPC in acetate buffer for 1 min is shown in Fig. 2a,c. The topography indicates structures whose diameters are greater than 20 nm for DOPC, generally round in shape and which are considerably larger for gram-AC2–DOPC vesicles. The lowest value for the diameter may be a result of the tip size being projected onto even smaller surface features [38]. Our tips have radii of curvature which average approximately 15 nm. From AFM images of gold nanospheres and scanning electron microscopic images of MAC-mode tips (data not shown), we are convinced that our tips have no significant protrusions. The heights of the features display are binary. That is, the heights of the small diameter surface features are 6 ± 1 nm and 12 ± 2 nm for pure DOPC and gram-AC2–DOPC liposome solution, respectively. These are suggestive of single and double bilayers. The 12 nm high features do not, however, appear to represent spherical vesicles. The features resemble oblate disks. The images of these features were stable over a period of a few hours, regardless of whether modified or unmodified mica was used. Occasionally, a single disk feature would disappear.

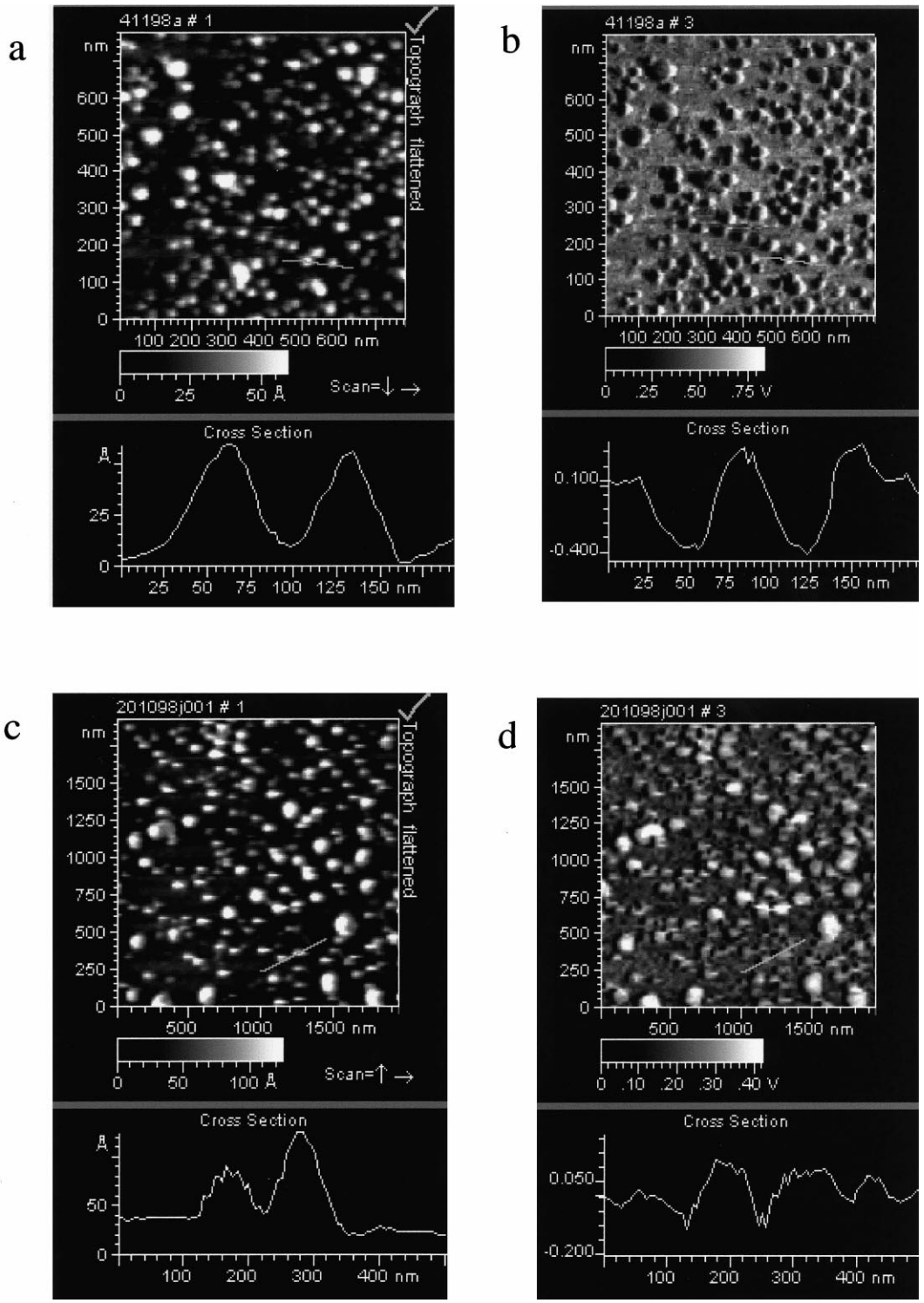

Fig. 2. The AFM topography and phase images of pure DOPC vesicles on a modified mica surface in aqueous solution, (a) and (b), respectively. The AFM topography and phase images of gramicidin-AC2 containing DOPC vesicles on a modified mica surface in aqueous solution, (c) and (d), respectively. The cross sections represent the light gray bar in the bottom left hand quadrant of the images.

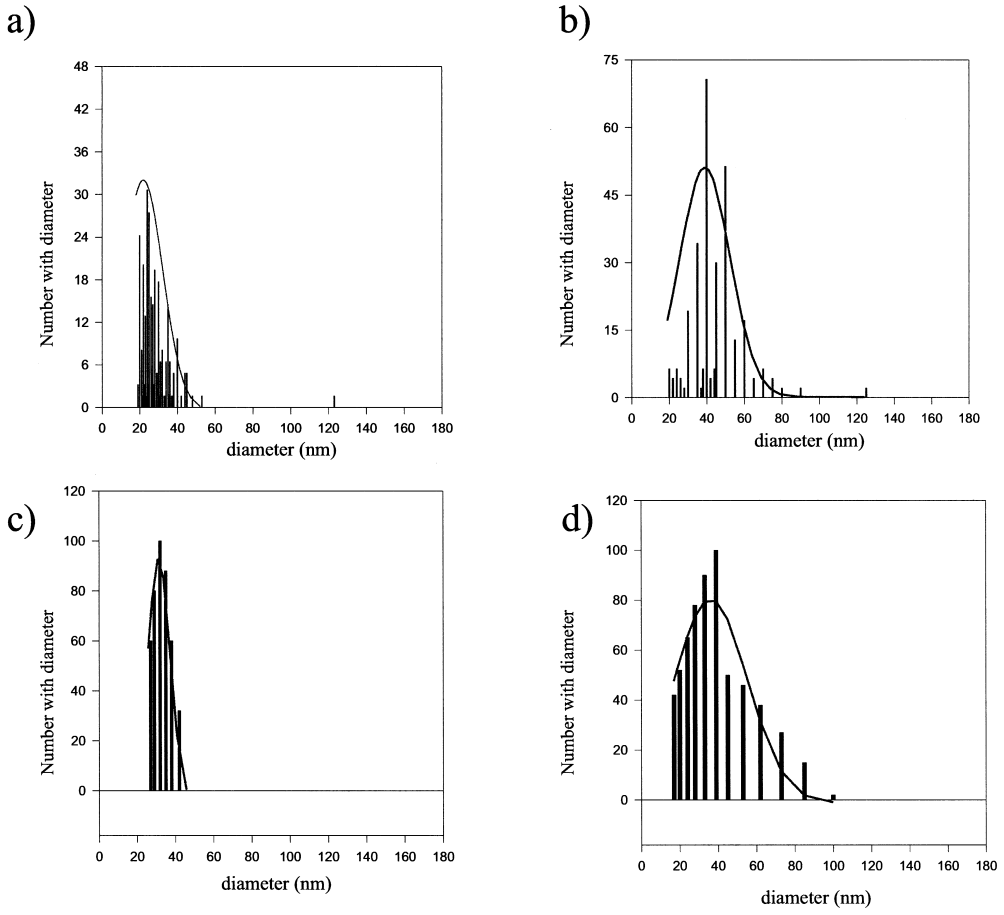

Fig. 3. Histograms generated from the analysis of the AFM images in Fig. 2. (a) and (b) are the distributions of vesicle diameters for the pure DOPC and gramicidin-AC2 containing vesicles, respectively. The solid lines represent the fit of a Gaussian distribution function to the data. Vesicle diameter histograms found from DLS on the pure DOPC (c) and gramicidin-AC2 (d) containing vesicles in acetate buffer. The solid lines represent the fit of a Gaussian distribution function to the data. The parameters for the fits can be found in Table 3.

The vesicle size distributions were analyzed statistically using a Gaussian function to determine the mean diameters (Fig. 3a,b). The results of this analysis are presented in Table 3. It is notable that the inclusion of gram-AC2 in the DOPC vesicles led to an increase in mean diameter of the surface features. For comparison with the vesicle size in solution, DLS was used to assess the solution size distribution.

Table 3

Sample	Diameter (nm)
DOPC (AFM)	22 ± 2
Gram-AC2–DOPC (AFM)	40 ± 3
DOPC (DLS)	30 ± 2
Gram-AC2–DOPC (DLS)	36 ± 2

The diameter histograms, determined from DLS, are presented in Fig. 3c,d. They compare favorably with the DOPC vesicles with gram-AC2 incorporated and less so for the pure DOPC vesicles.

Exposing modified and unmodified mica to a solution with the same concentration of phospholipid resulted in considerably different vesicle deposition rates. To obtain the surface density shown in the AFM image in Fig. 2a, a 0.1 mg/ml DOPC solution with a deposition time of 2 min was used for modified mica and 0.2 mg/ml DOPC solution with 5 min was used for unmodified mica. These deposition rates suggest that the vesicles need fewer collisions with the modified surface to adsorb. This may indicate that the adsorption step is more favorable energetically for the modified mica surface, since surface

modification was the only change between the two experiments.

By using the phase image from MAC–AFM, we can uniquely confirm that we observe the mica substrate between the DOPC features. The MAC mode phase image represents the difference between the oscillating magnetic field driving the tip and its true response. As the tip encounters a soft object, its oscillations will be damped and phase-shifted. Thus, changes in phase should occur as the tip encounters the side of a liposome and then change again as it scans over the liposome surface. A phase image is shown for pure DOPC vesicles in Fig. 2b. One can see that the phase change is the greatest at the vesicle edge and then recovers as the tip scans across the surface where it experiences a more pliant material.

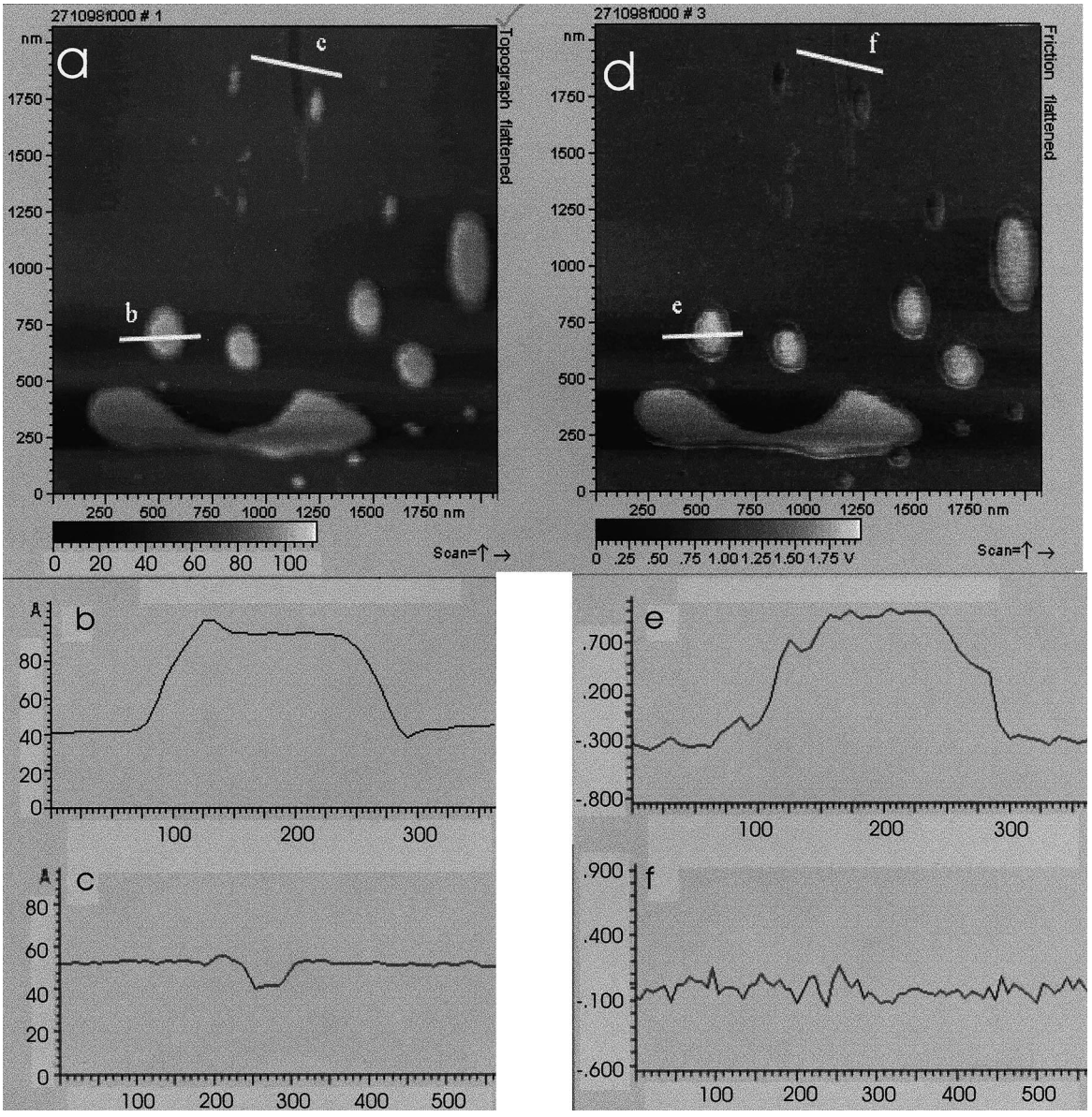

Fig. 4. AFM image of intermediate stage of SPB formation. The sample was prepared from a 0.2 mg/ml solution of DOPC in acetate buffer. The unmodified mica surface was exposed to the solution for 5 min and then rinsed with ultrapure deionized water. The sample was imaged in ultrapure water. (a) A topographical image. (b) and (c) The cross-section indicated by lines (b) and (c) in panel (a), respectively. (d) A phase contrast image recorded simultaneously with the image in panel (a). (e) and (f) The phase cross-sections associated with lines (e) and (f) in panel (a).

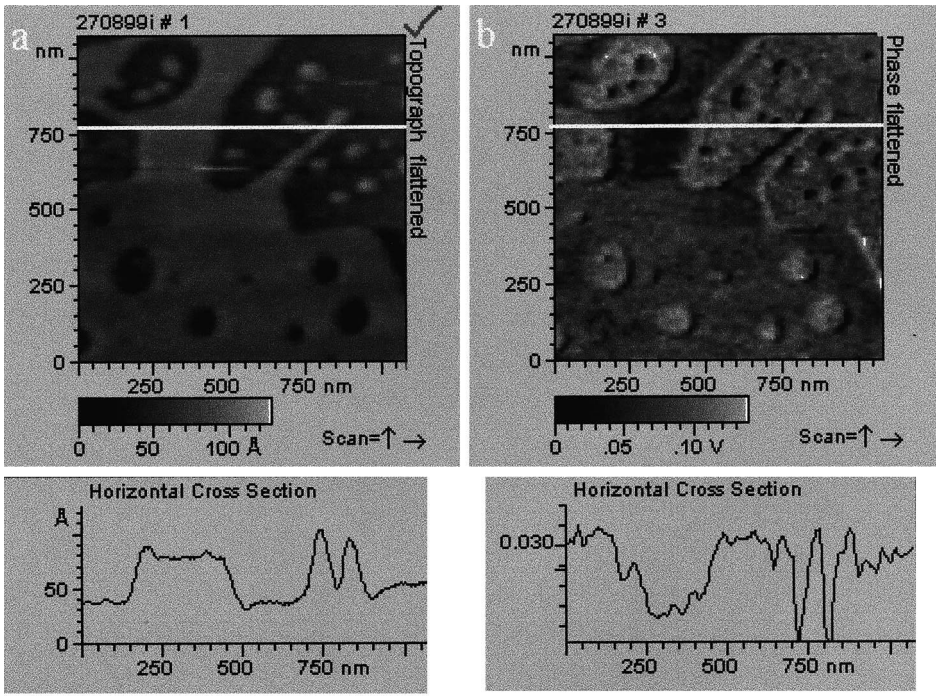

Fig. 5. AFM image of intermediate stage of SPB formation. The sample was prepared from a 0.2 mg/ml solution of DOPC in acetate buffer. The APTES-modified mica surface was exposed to the solution for 1.5 min and then rinsed with ultrapure deionized water. The sample was imaged in ultrapure water. (a) The topographical image including the height cross-section indicated by the horizontal line. (b) The phase contrast image including the phase cross-section indicated by the horizontal line.

The height (i.e. damping) response may be less sensitive to these elasticity changes in the vesicle's surface. We have observed that the phase images almost always provide equivalent or better contrast compared with the topographical images. There is a significant difference in the phase images of pure DOPC and gramicidin-AC2 containing vesicles as shown in Fig. 2b,d, suggesting that these features have different friction coefficients. This is mainly owing to the wider range of phase contrast for the image of pure DOPC compared with that of gram-AC2–DOPC. The phase of modulation is related to the elasticity and adhesion of the surface to the AFM tip [31,39]. The wider range for pure DOPC indicates that the surfaces of these vesicles are more adhesive to the AFM tip and/or more elastic than those containing the lipophilic polypeptide gram-AC2. This would be consistent with a repacking of phospholipids around gramicidin leading to a lowering of membrane fluidity. The lowering of elasticity is also consistent with the re-emerging theory that general anesthesia results from lipophilic molecules which induce changes in membranes making them more rigid [40].

In Fig. 4, we present a striking example of the power of phase contrast in MAC–AFM. The image is of a 0.2 mg/ml DOPC sample exposed to unmodified mica for 10 min. This results in intermediate regime in surface coverage where there is some continuous coverage and some disks (see Section 3.2). In this image, we draw attention to two features; one near the top and one in the bottom left quadrant of Fig. 4a. The bottom left indicates a large feature of height appropriate for a bilayer (see cross-section in Fig. 4b). The contrast in the phase image shows up nicely for this feature (see Fig. 4d,e). We can compare this with the feature near the top of the image. This indentation is typical for a defect in the mica surface. These defects result from imperfect cleavage. Its height difference is considerably less than the disk (see Fig. 4a,c for cross-section). Note that in the phase image, Fig. 4d,f, this feature is essentially absent indicating that it has the same friction characteristics as unmodified mica. This confirms that the feature is simply a defect in the mica surface. We have observed these features on pure mica surfaces (data not shown) which have not been exposed to DOPC

solution, with the same lack of significant phase difference. Given the above observations, we are confident that the phase images in MAC–AFM allow us to make the distinction between areas of no coverage and areas covered with phospholipid. Phase contrast will be exploited to interpret the AFM images collected during the later stages of SPB formation.

3.2. Intermediate stage: partial bilayer coverage

With increasing time of liposome solution exposure, for example 1 min 30 s for 0.2 mg/ml DOPC solutions on modified mica, the surface features change indicating the initiation of vesicle fusion. Here we observe areas of both single disk features and of homogeneous coverage. The width and height of the single disk features follow the same statistics

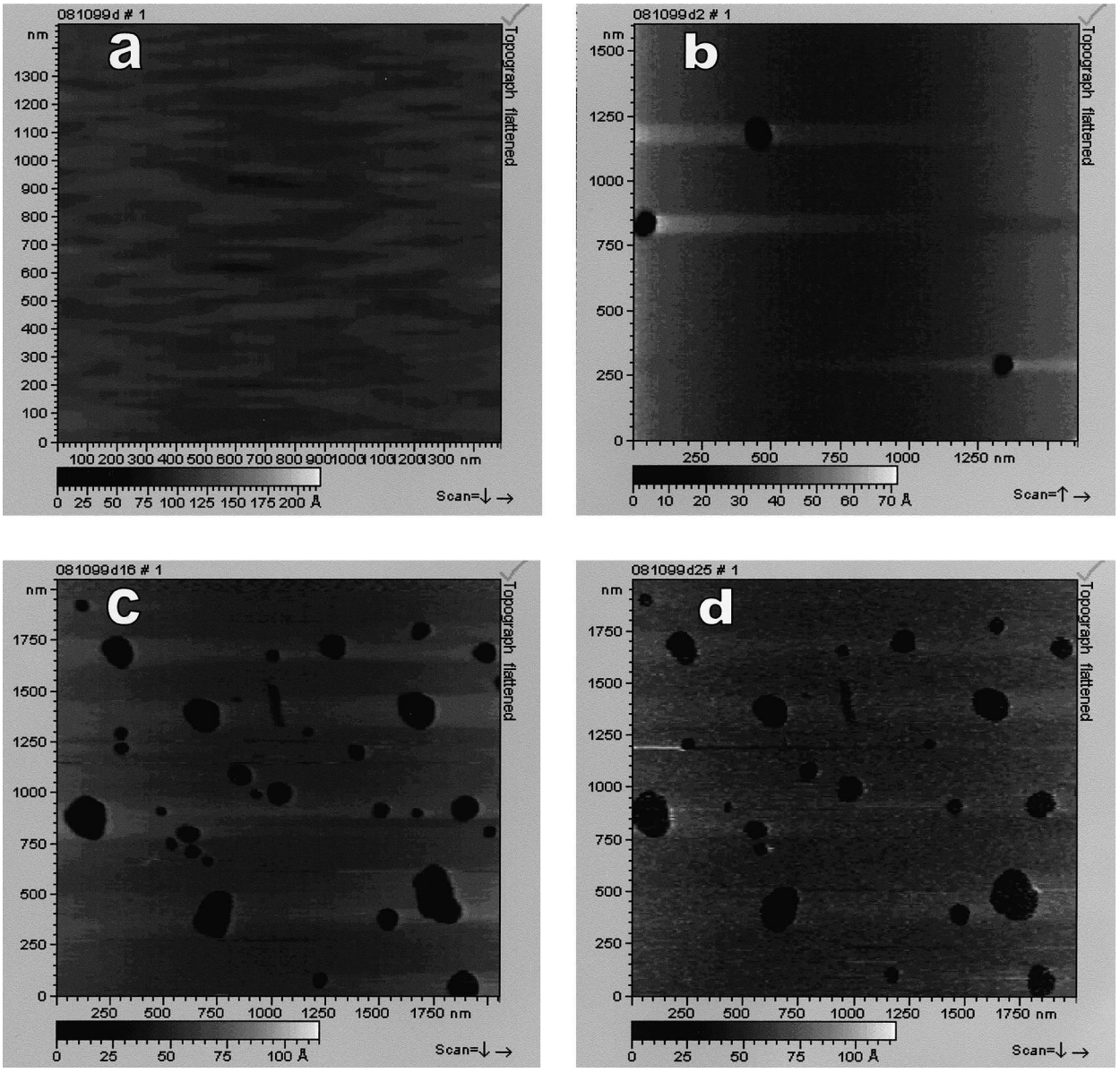

Fig. 6. AFM image of the final stage of SPB formation. The sample was prepared from a 0.2 mg/ml solution of DOPC in acetate buffer. The APTES-modified mica surface was exposed to the solution for 2 min and then rinsed with ultrapure deionized water. (a) The sample shortly after preparation (approximately 10 min). (b) Collected 1 h after the image in (a). (c) Collected 5 h after the image in (a). (d) Collected 6 h after the image in (a).

as at earlier exposure times. The area of continuously covered surface has a height of 6 ± 1.5 nm, measured at its edges. We display a typical image in Fig. 5. Included here are both topography and phase (friction). Because the contrast in the phase scan is so striking, we submit that the surface features represent two different materials. These materials are most likely DOPC and neat modified mica. Note that compared with Fig. 4 the surface coverage is much more extensive.

A comparison for gram-AC2–DOPC versus DOPC at intermediate stage of coverage reveals that, although the deposition is slower in the former case, the same AFM features indicating partial coverage become visible.

3.3. Final stage: complete bilayer coverage

For exposure times of 2 min or greater for 0.2 mg/ml DOPC and 0.5 mg/ml gram-AC2–DOPC nearly complete coverage of the modified mica surface was observed. In many instances the completeness of the coverage was limited by small surface defects appearing as indentations or holes. A characteristic example of this is shown in Fig. 6a–d. The hole depth is measured at 6 ± 1.5 nm. This depth, in addition to the high contrast phase scans, led us to suspect that we observed a complete bilayer with holes one bilayer thick at the bottom of which is mica. The gram-AC2 sample was more prone to surface defects immediately upon imaging, whereas the pure DOPC often appeared as a homogeneous bilayer which developed defects with time. We observed defect formation regardless of whether or not we were scanning continuously and therefore assume that this phenomenon is not related to probe–surface interactions.

3.4. Bilayer dynamics

As suggested above, when we imaged the final stage in SPB formation via vesicle fusion, we observed the supported bilayer to be quite dynamic. In Fig. 6a–d) we show a surface completely covered with DOPC, which after 60 min develops 6 nm deep surface defects. When less than 100 nm in diameter, the vast majority of these defects are circular in shape. As they become larger, they begin to take on more elongated shapes. Moreover, the holes themselves are quite dynamic. After approximately 90 min, the total surface area of the defects reaches a steady state, but there is continual annihilation and generation of the smaller holes. An example of this form of bilayer dynamics is exhibited in Fig. 7a–c. In this figure, we were able to triangulate the position on the surface using the three larger holes shown by arrows. Over the 5 h total imaging time, many of the smaller features nearby these defects either disappear or fuse to form larger defects.

4. Discussion

4.1. Vesicle deposition

An interesting question to ask is whether or not the vesicles deposited on the mica surface represent an adhesion event for every surface–liposome collision. When the drop of vesicle solution is first gently placed on the mica surface there may be turbulence owing to the flow of solution as it wets the surface. However, this turbulence should damp out rapidly as the system re-establishes an equilibrium temperature [41]. In the following, we will estimate the number of liposome–surface collisions assuming that any initial turbulence has been damped within a few seconds. Using a DOPC concentration of 2.6×10^{-3} M and an average aggregation number of 4000 phospholipids/vesicle, we obtain a vesicle concentration of 4.24×10^{20} vesicles/m^3. If we consider a simple projection of this density of vesicles onto a 1 μm square surface (with 1 μm height), an instantaneous surface density of 424 vesicles/μm^2 is realized. We measure an average of 150 vesicles/μm^2 on the surface, after a 2 min exposure and a brief rinse with ultrapure water. During a 2 min deposition time, the fastest moving (i.e. smallest) vesicles travel, on average, 51 μm. This was calculated assuming random diffusion and a Stokes–Einstein diffusion coefficient of 1.1×10^{-11} m^2/s. Thus, 21 000 vesicles could interact with the surface over the deposition time. This analysis indicates it is unlikely that every vesicle–surface interaction results in adhesion.

What then are the forces holding the bilayer to the surface? Firstly, from a chemical potential point of view, a liquid phase DOPC bilayer (the phase transition temperature is −22°C) is in its most stable

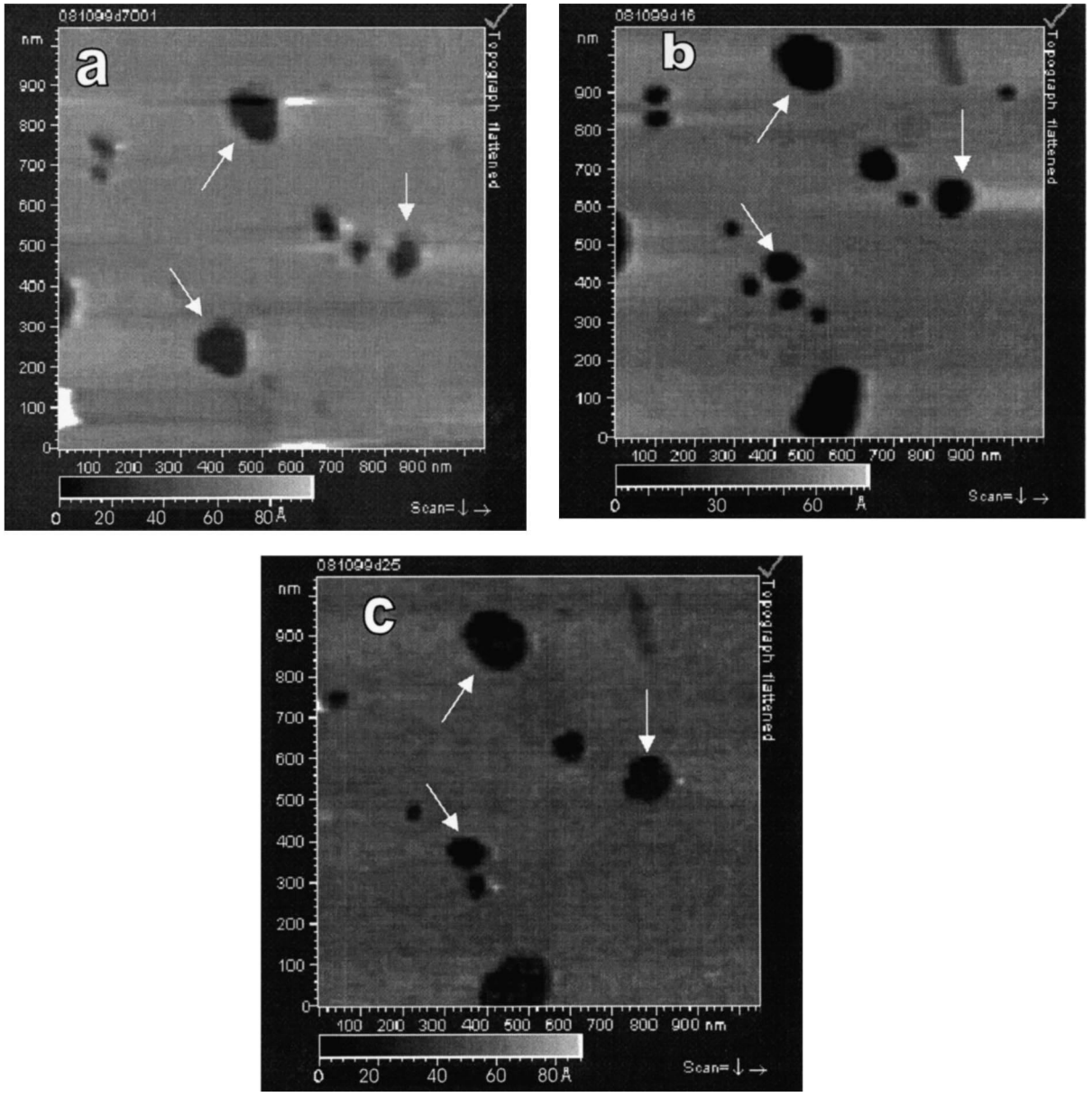

Fig. 7. Dynamics of the DOPC bilayer. AFM image of the final stage of SPB formation. The sample was prepared from a 0.2 mg/ml solution of DOPC in acetate buffer. The APTES-modified mica surface was exposed to the solution for 2 min and then rinsed with ultrapure deionized water. (a) The sample 180 min after preparation. (b) Collected 30 min after the image in (a). (c) Collected 1 h and 30 min after the image in (a). The arrows indicate the same three surface defects. Note the changing features near these defects.

configuration when planar. Any planar, inert surface will provide a template for this to occur. Thus, vesicles in solution will always have a tendency to deposit onto a surface and flatten out [27,28]. In order to remain on the surface, the energy advantage must not be offset by any repulsion energy between the surface and the phospholipid. This repulsion could arise from like-charge Coulomb interactions, for example. We find that unmodified mica will support either a DOPC or a gram-AC2–DOPC bilayer. In aqueous solution at neutral pH, the surface of mica is known to have a negative charge owing to the mismatch between the sublayer of OH^- (complexed to Al) and the surface bound K^+ ions [31]. An electrostatic binding is possible due to the zwitterionic nature of the DOPC head group. The pos-

itive tri-methyl quaternary amino moiety in the head group could be oriented such that it is closer to the negative surface than the negative phosphate. It is well established that the head groups of phospholipids interact with mica surfaces mediated by a thin layer of water [19,20]. This hydration layer could account for the good agreement between the well-hydrated DOPC D-spacing of 6.3 nm measured using X-ray diffraction and our height of 6 ± 1.5 nm [42]. Thus, this apparent hydration layer would be slightly thinner than other groups have suggested for similar systems. For example Johnson et al. [43] suggest 1–2 nm for a dimyristoylphosphatidylcholine bilayer measured with specular reflection of neutrons and 1 nm suggested by Beckmann et al. [17] for 1,2-dipentadecanoyl-*sn*-glycero-3-phosphocholine on silicon.

Modification of the surface using APTES results in more favorable adhesion for DOPC vesicles given the decrease in exposure time needed for surface coverage. The modification increases the surface positive charge owing to the amine group, which is protonated at neutral pH. Thus, coverage of the mica surface by APTES results in the surface attaining a net positive charge [31]. Here, the negative phosphate moiety in the DOPC head group could be oriented such that it is closer to the negative surface than the positive tri-ethyl amino group. The more favorable attraction may result from the natural tendency of the DOPC head group to project this orientation.

The inclusion of gramicidin-AC2 in the liposomes makes them less surface adhesive. Therefore, gram-AC2 must reduce the favorable interaction energy. Gramicidin ion channels will decrease the hydrophilicity of a bilayer by displacing DOPC molecules. Additionally, the displacement of phospholipid head groups by the ion channels necessarily means a disruption in the ordering of the hydration layer between a bilayer and its supporting surface. Indeed, Lundbaek et al. [44] suggest that local membrane curvature exists at the gramicidin–lipid interface.

We now consider the formation of the single bilayer disk features. Energetically favorable DOPC–surface interactions will cause the liposomes to flatten on the surface. However, if the vesicles only flattened, then one should observe surface features which have a minimum height of two bilayers or 12 nm. This would assume that the solution inside the vesicle is either compressible or could partially vacate the interior. The vast majority of the features observed are approximately 6 nm suggesting that the vesicles have ruptured and that single bilayer disks result. The rupture could result from the following phenomena. Buffer may be trapped within surface-bound vesicles as a result of the washing process. This may result in some osmotic pressure exerted on the vesicle membrane. For the concentration of buffer used, the pressure would be a maximum of 0.25 atmosphere if the bilayer was impermeable to all acetate buffer components. According to the Boyle Van 't Hoff Law, there would be a maximum of a 14% gain in vesicle diameter, compared with vesicles in an isotonic solution [45]. This plus mechanical stress during rinsing will probably cause lysis of the vesicles leading to single bilayer formation. Our observation of almost exclusively disk features for pure DOPC is in contrast with that of Reviakine and Brisson [26]. In their work they sometimes observed intact vesicles on a mica surface. We believe the difference is in the sample preparation for imaging. We rinsed with pure water whereas they exchanged the vesicle solution with pure buffer. In some instances, Reviakine and Brisson observed solely bilayers when rinsing more frequently or with a buffer of different ionic strength.

Once ruptured, the tendency of the bilayer to become completely flat can be fulfilled and the dangling 'flaps' of the ruptured vesicle can adsorb to the surface. We present a cartoon of this process in Fig. 8, modeled after the proposed mechanism of Rädler et al. [19] and Puu and Gustafson [22]. This includes the proposed disk boundary structure, where the

→

Fig. 8. The proposed mechanism of the first stage of supported bilayer formation via vesicle fusion. The cartoon represents cross-sections through phospholipid structures. (a) The vesicle is flattened because of interactions with the surface. Also indicated are potential rupture lines in the vesicle. (b) The vesicle ruptures owing to mechanical and osmotic stress. The dangling flaps of the ruptured vesicle migrate to the surface. (c) A single bilayer is formed. The phospholipids reorganize at the edges of the disk in order to minimize hydrophobic interactions.

a

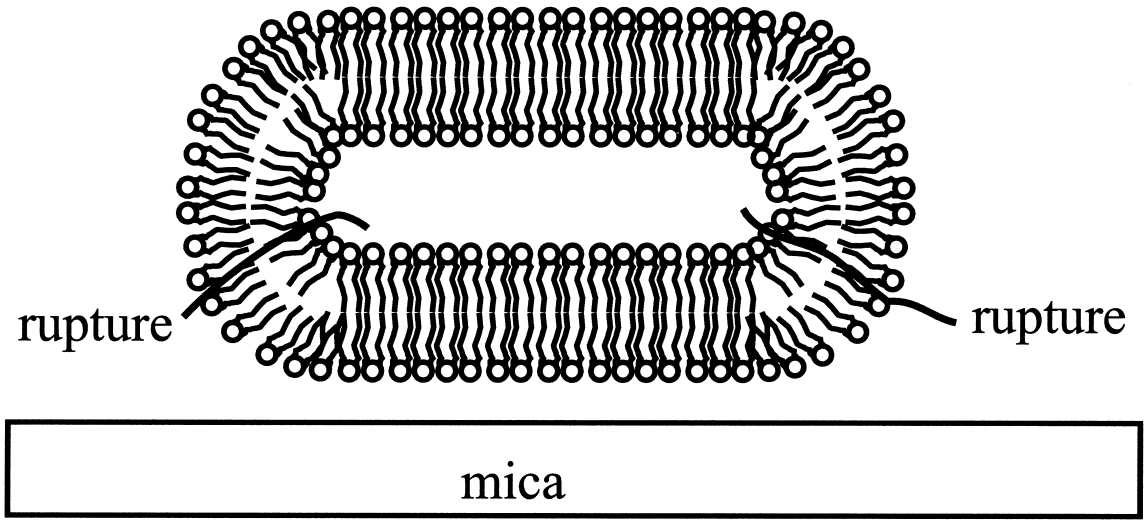

b

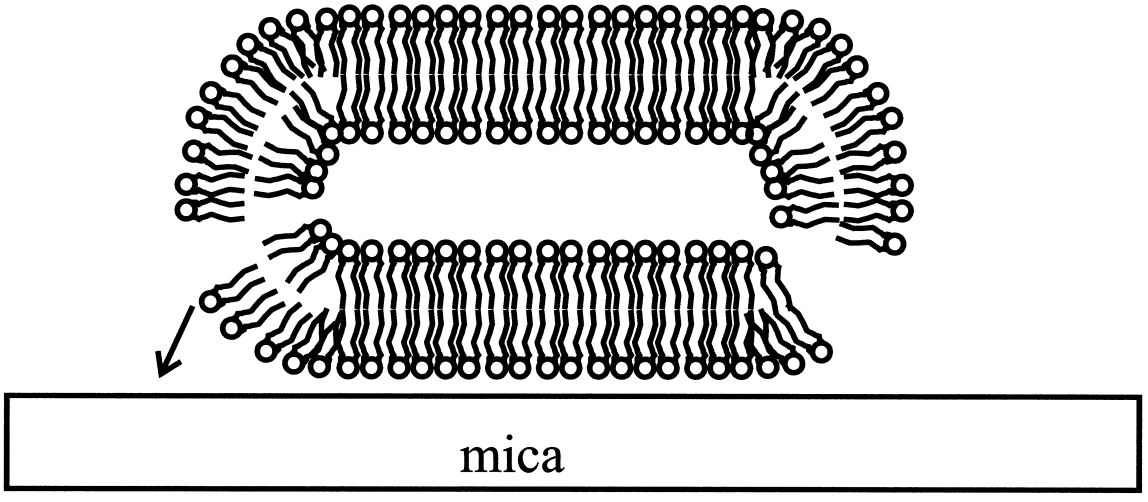

c

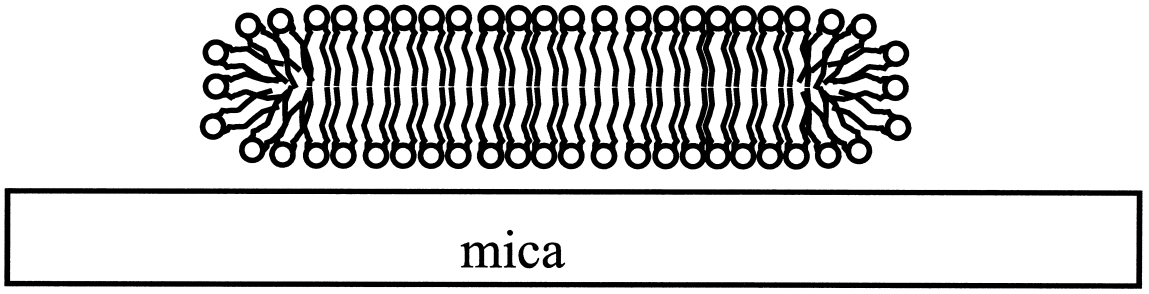

DOPC molecules reorient in order to minimize the exposure of the lipid chains to the surrounding water. The radii of the disks will depend on the rupture sites, which are not necessarily on opposite sides of the bound vesicles. Moreover, the mechanical perturbation of our rinsing step in the bilayer preparation may lead to multiple rupture sites. Thus, rupture sites close together could account for the smaller radii of the adsorbed disks compared with the free vesicles in solution.

The single circular entities for gram-AC2–DOPC behave in much the same way as pure DOPC with the exception that we observe many features with a 12 nm height. This is indicative of either a severely flattened intact vesicle or a double bilayer. We can speculate that the inclusion of the ion channel in the membrane may lead to stiffening of the membrane and/or to some ability to relieve osmotic stress. In this case a flattened vesicle could remain intact on the surface.

It is not surprising that the circular bilayer features found in the early stage of deposition are very stable. A concerted phospholipid motion necessary for an entire disk to move would be highly unlikely in the absence of some driving force. At this stage in the supported bilayer formation, one would observe corralled diffusion with a distribution of corral sizes based on the size distribution of the disks. We would expect to observe no free diffusion until significant areas are continuously covered. Indeed, such behavior has been previously observed for 1-palmitoyl-2-oleoyl-*sn*-glycero-3-phosphocholine (POPC) vesicle adsorption to quartz, measured using TIR–FRAP [12]. In their work, Kalb et al. [12] observed no free diffusion of POPC until a complete bilayer was formed. The TIR–FRAP measurements would be sensitive only to diffusion on a length scale of μm. Thus, they would not be sensitive to the intra-disk phospholipid motion, during the early stage of vesicle deposition.

4.2. Vesicle fusion

The AFM images of the intermediate stage of bilayer formation (see Fig. 5 for example) may provide some insight into the mechanism of surface fusion to form the supported bilayers observed in this work. For fusion of the deposited DOPC vesicles/disks, the fusion seems to occur before disk formation. The apparent fast rate of bilayer formation that we observe for DOPC (i.e. within a few minutes) is in keeping with the findings of Puu and Gustafson [22] for DOPC adsorption onto a silicon–nitride surface. This is because we observe disk-like structures in close proximity that are not fused. If there was a strong propensity for fusion of proximal disks, then we would expect to see more continuous bilayer features even at lower vesicle concentration. Moreover, since we do not observe significant regimes of double bilayer height (i.e. 12 nm), there appears to be a lower adsorption propensity for vesicles that encounter a preformed bilayer.

The stability of the images in the early and intermediate stages of liposome deposition suggests that for both DOPC and gram-AC2–DOPC, extended bilayers do not form as a result of disk migration. Rather the surface 'fills in' as more liposomes adsorb. From the intermediate stage images, it appears that fusion of proximal disks/liposomes is almost immediate. This is apparent from Fig. 5 (pure DOPC), where there are two domains; one with continuous coverage and one with single disk entities. The inclusion of gramicidin-AC2 in the liposomes appears to affect only the rate of bilayer formation, but not the mechanism. Some characteristic of the gram-AC2–DOPC liposomes is evidently slowing down the fusion process. Unlike the work of Mou et al. [46], we observe no evidence of a gramicidin-induced phospholipid phase change. This is probably because we employed a lower gramicidin/DOPC ratio than used in reference [46]. For the formation of a complete supported bilayer, we have observed no evidence of phase boundaries for either DOPC or DOPC–gram-AC2 bilayers. Additionally, the affect of modified versus unmodified mica is only on the bilayer formation rate and not the mechanism.

4.3. SPB dynamics

From the time series of images presented in Fig. 6, it is apparent that the complete bilayer eventually develops defects. These defects begin as circular holes, grow in size and number and finally reach a steady state distribution. The defects provide us with the serendipitous ability to measure the height of the surface DOPC layer. Additionally, the phase contrast

between the DOPC layer and the bottom of the defect strongly suggests that the bottom is a different material, namely the (modified) mica substrate. Defects in SPBs have been observed previously in supported phospholipid bilayers using both AFM of both symmetric and asymmetric phosphatidylethanolamine bilayers [15] and of 1,2-dipentadecanoyl-*sn*-glycero-3-phosphocholine on mica [17] and of DOPC bilayers and dimyristoylphosphatidylcholine (DMPC) bilayers on silicon wafers using fluorescence microscopy [11]. In the present study, we observe defect formation regardless of whether we are continuously imaging the sample or not. Therefore, this process is independent of tip–surface interactions. This is in contrast with contact mode AFM studies of SPBs where the AFM tip was found to modify the soft phospholipid bilayer [17,26]. In fact, over a 6 h scanning period using MAC we never observed tip-induced surface modifications. The rate of defect formation and the steady state defect dynamics however do depend on inclusion of gramicidin in the DOPC liposomes. Both of these phenomena are slower in gram-AC2–DOPC samples consistent with a protein-induced stiffening of the membrane.

Defect formation probably results from instantaneous local differences in DOPC bilayer density that led to local differences in lateral bilayer pressure and put the bilayer under tension. If this tension is insurmountable, local ruptures are generated in the bilayer. These ruptures may assume a circular structure to minimize the surface tension of the nascent bilayer boundary. The defect shapes that we observe are in striking resemblance to those predicted and observed by Gallez and McConnell [47] for monolayers of DMPC with 10 mol% gramicidin on microscope coverglass. Moreover, Tamm and McConnell [11] have shown that large (20–40 μm diameter) surface defects can be induced in DOPC bilayers by lowering the sample temperature, but not below the phase transition. They suggest that this would lead to a highly localized lipid chain condensation that may be the driving force behind defect formation. Similar to the larger defects we have observed, the defects they observed never collapsed. In contrast, the smaller defects we observed are relatively dynamic as is apparent from Fig. 7. Thus, for the smaller defects (i.e. 100 nm diameter and below) there must be a fine balance between the gain in negative free energy by minimizing surface tension and the instability caused by the DOPC reorientation at the bilayer boundaries.

The 'fast' dynamic behavior of the smaller defects is relative, since we observed nm scale changes that occurred over a period of tens of minutes to hours. If free diffusion was driving the process, then the crossing time over a 50 nm defect would be on the order of ms. This can be estimated using the surface diffusion coefficient of approximately 5×10^{-12} m^2/s determined for dimyristoylphosphatidylethanolamine (DMPE) in a supported 1-palmitoyl-2-oleoyl-*sn*-glycero-3-phosphatidylethanolamine/POPC bilayer [3]. Moreover, the dynamics we observe are still much slower than the bilayer spreading dynamics observed by Nissen et al. [20] for DMPC on mica (43 $\mu m^2/s$) and by Cremer and Boxer [48] for egg-PC on silica (front advance rate of 1–10 μm/s). Presumably there is a much weaker driving force for the formation and healing of the defects we observe. Therefore, the dynamics must result from a combination of free and hindered diffusion, with the lateral diffusion at the defect boundary being very slow. This would suggest anomalous diffusion behavior that could be measured for a 'macroscopically complete' bilayer.

It is probable that the images presented here can be extrapolated to the general phenomenon of SPB formation via vesicle fusion. The incorporation of a simple polypeptide into the vesicles affects only the rate of bilayer deposition, and perhaps also the resilience to rupture. We have observed the spontaneous formation of stable defects in the bilayers. Again, only the rate of defect formation and their dynamic distribution are affected by the incorporation of protein into the vesicles. Through our work, we hope to have provided a better sense of the advantages and limitations of vesicle fusion for SPB formation.

Acknowledgements

The authors would like to thank Professor G.A. Woolley (University of Toronto) for the kind donation of gramicidin-AC2 samples. T.M. Duchscherer (University of Calgary) helped in the preparation of some liposome solutions. We thank Professor Stephanie Tristram-Nagle and Dr. Neil Warrender for many helpful discussions. We are indebted to Professor G. Liu (University of Calgary) for the use of his

DLS apparatus. Financial support from the Natural Sciences and Engineering Research Council of Canada, the University of Calgary, the Intellectual Infrastructure Partnership Program (Government of Alberta), and Travis Chemicals (Division of Stanchem) is gratefully acknowledged. The authors are indebted to Molecular Imaging for their continuing support.

References

[1] H.M. McConnell, T.H. Watts, R.M. Weiss, A.A. Brian, Supported planar membranes in studies of cell–cell recognition in the immune system, Biochim. Biophys. Acta 864 (1986) 95–106.
[2] M. Stelze, E. Sackmann, Sensitive detection of protein adsorption to supported lipid bilayers by frequency dependent capacity measurements and microelectrophoresis, Biochim. Biophys. Acta 981 (1989) 135–142.
[3] A. Sonnleitner, G.J. Schutz, Th. Schmidt, Free Brownian motion of individual lipid molecules in biomembranes, Biophys. J. 77 (1999) 2638–2642.
[4] E. Kalb, J. Engel, L.K. Tamm, Binding of proteins to specific target sites in membranes measured by total internal reflection fluorescence microscopy, Biochemistry 29 (1990) 1607–1613.
[5] A. Schmidt, J. Spinke, T. Bayerl, E. Sackmann, W. Knoll, Streptavidin binding to biotinylated lipid layers on solid supports, Biophys. J. 63 (1992) 1185–1192.
[6] J.J. Ramsden, P. Schneider, membrane insertion and antibody recognition of a glycosylphosphytidylinositol-anchored protein an optical study, Biochemistry 32 (1993) 523–529.
[7] K.H. Pearce, R.G. Hiskey, N.L. Thompson, Surface binding kinetics of prothrombin fragment 1 on planar membranes measured by total internal reflection fluorescence microscopy, Biochemisty 31 (1992) 5983–5995.
[8] L.K. Nielsen, J. Risbo, T.H. Callisen, T. Bjornholm, Lagburst kinetics in phospholipase A_2 hydrolysis of DPPC bilayers visualized by atomic force microscopy, Biochim. Biophys. Acta 1420 (1999) 266–271.
[9] D. Bizzotto, A. Nelson, Continuing electrochemical studies of phospholipid monolayers of dioleoyl phosphatidylcholine at the mercury-electrolyte interface, Langmuir 14 (1998) 6269–6273.
[10] A. Nelson, D. Bizzotto, Chronoamperometric study of Ti(I) reduction at gramicidin-modified phospholipid-coated mercury electrodes, Langmuir 15 (1999) 7031–7040.
[11] L.K. Tamm, H.M. McConnell, Supported phospholipid bilayers, Biophys. J. 47 (1985) 105–113.
[12] E. Kalb, S. Frey, L.K. Tamm, Formation of planar bilayers by fusion of vesicles to supported phospholipid monolayers, Biochim. Biophys. Acta 1103 (1992) 307–316.
[13] P. Nollert, H. Kiefer, F. Jahnig, Lipid vesicle adsorption versus formation of planar bilayers on solid surfaces, Biophys. J. 69 (1995) 1447–1455.
[14] J.A.N. Zasadzinski, C.A. Helm, M.L. Longo, A.L. Weisenhorn, S.A.C. Gould, P.K. Hansma, Atomic force microscopy of hydrated phosphatidylethanolamine bilayers, Biophys. J. 59 (1991) 755–760.
[15] S.W. Hui, R. Viswanathan, J.A. Zasadzinski, J.N. Israelachvili, The structure and stability of phospholipid bilayers by atomic force microscopy, Biophys. J. 68 (1995) 171–178.
[16] S. Singh, D.J. Keller, Atomic force microscopy of supported planar membrane bilayers, Biophys. J. 60 (1991) 1401–1410.
[17] M. Beckmann, P. Nollert, H.-A. Kolb, Manipulation and molecular resolution of a phosphatidylcholine-supported planar bilayer by atomic force microscopy, J. Membr. Biol. 161 (1998) 227–233.
[18] A.A. Brian, H.M. McConnell, Allogeneic stimulation of cytotoxic T cells by supported planar membranes, Proc. Natl. Acad. Sci. USA 81 (1984) 6159–6163.
[19] J. Rädler, H. Strey, E. Sackmann, Phenomenology and kinetics of lipid bilayer spreading on hydrophilic surfaces, Langmuir 11 (1995) 4539–4548.
[20] J. Nissen, S. Gritsch, G. Wiegand, J.O. Rädler, Wetting of phospholipid membranes on hydrophilic surfaces – concepts towards self-healing membranes, Eur. Phys. J. B 10 (1999) 335–344.
[21] C.A. Keller, B. Kasemo, Surface specific kinetics of lipid vesicle adsorption measured using a quartz crystal microbalance, Biophys. J. 75 (1998) 1397–1402.
[22] G. Puu, I. Gustafson, Planar lipid bilayers on solid supports from liposomes – factors of importance for kinetics and stability, Biochim. Biophys. Acta 1327 (1997) 149–161.
[23] R.G. Crystal, Transfer of genes to humans early lessons and obstacles to success, Science 270 (1997) 404–410.
[24] C. Le Grimellec, E. Lesniewska, M.-C. Giocondi, E. Finot, V. Vie, J.-P. Goudonnet, Imaging of the surface of living cells by low-force contact-mode atomic force microscopy, Biophys. J. 75 (1998) 695–704.
[25] E. A-Hassan, W.F. Heinz, M.D. Antonik, N.P. D'Costa, S. Nageswaran, C.-A. Schoenenberger, J.H. Hoh, Relative microelastic mapping of living cells by atomic force microscopy, Biophys. J. 74 (1998) 1564–1578.
[26] I. Reviakine, A. Brisson, Formation of supported phospholipid bilayers from unilamellar vesicles investigated by atomic force microscopy, Langmuir 16 (2000) 1806–1815.
[27] R. Lipowsky, U. Seifert, Adhesion of vesicles and membranes, Mol. Cryst. Liq. Cryst. 202 (1991) 17–25.
[28] U. Seifert, Configurations of fluid membranes and vesicles, Adv. Phys. 46 (1997) 13–137.
[29] B. Pignataro, C. Steinem, H.-J. Galla, H. Fuchs, A. Janshoff, Specific adhesion of vesicles monitored by scanning force microscopy and quartz crystal microbalance, Biophys. J. 78 (2000) 487–498.
[30] D.J.C. Jaikaran, Z. Zhang, G.A. Woolley, C-terminal amino groups facilitate membrane incorporation of gramicidin derivatives, Biochim. Biophys. Acta 1234 (1995) 133–138.
[31] S.M. Lindsay, Y.L. Lyubchenko, N.J. Tao, Y.Q. Li, P.I.

Oden, J.A. De Roo, J. Pan, Scanning tunneling microscopy and atomic force microscopy studies of biomaterials at a solid–liquid interface, J. Vac. Sci. Technol. A 11 (1993) 808–816.
[32] Y.L. Lyubchenko, L.S. Shlyakhenko, Visualization of supercoiled DNA with atomic force microscopy in situ, Proc. Natl. Acad. Sci. USA 94 (1997) 496–501.
[33] D.J. Muller, M. Amrein, A. Engel, Adsorption of biological molecules to a solid support for scanning probe microscopy, J. Struct. Biol. 119 (1997) 172–188.
[34] P. Trens, R. Denoyel, J. Rouquerol, Adsorption of (γ-aminopropyl)triethoxysilane on silica from aqueous solution: A microcalorometric study, Langmuir 11 (1995) 551–554.
[35] W. Han, S.M. Lindsay, T. Jing, A magnetically driven oscillating probe microscope for operation in liquids, Appl. Phys. Lett. 69 (1996) 1–3.
[36] W. Han, S.M. Lindsay, Probing molecular order at a liquid–solid interface with a magnetically oscillated atomic force microscope, Appl. Phys. Lett. 72 (1998) 1656–1658.
[37] J. Ding, G. Liu, Polystyrene-block-poly(2-cinnamoylethyl methacrylate) nanospheres with cross-linked shells, Macromolecules 31 (1998) 6554–6558.
[38] J. Vesenka, S. Manne, R. Giberson, T. Marsh, E. Henderson, Colloid gold particles as an incompressible atomic force microscope imaging standard for assessing the compressibility of biomolecules, Biophys. J. 65 (1993) 992–997.
[39] S.K. Rhee, A.P. Quist, R. Lal, Amyloid β protein-(1-42) forms calcium permeable, Zn^{2+} selective channel, J. Biol. Chem. 272 (1998) 13379–13382.
[40] K. Tu, M. Tarek, M.L. Klein, D. Scharf, Effects of anesthetics on the structure of a phospholipid bilayer: molecular dynamics investigation of halothane in the hydrated liquid crystal phase of dipalmitoylphosphatidylcholine, Biophys. J. 75 (1998) 2123–2134.
[41] T. Cebeci, A.M.O. Smith, Analysis of Turbulent Boundary Layers, Academic Press, New York, 1974.
[42] S. Tristram-Nagle, H.I. Petrache, J.F. Nagle, Structure and interactions of fully hydrated dioleoylphosphatidylcholine bilayers, Biophys. J. 75 (1998) 917–925.
[43] S.J. Johnson, T.M. Bayerl, D.C. McDermott, G.W. Adam, A.R. Rennie, R.K. Thomas, E. Sackmann, Structure of an adsorbed dimystroylphosphatidylcholine bilayer measured with specular reflection of neutrons, Biophys. J. 59 (1991) 289–294.
[44] J.A. Lundbæk, A.M. Maer, O.S. Andersen, Lipid bilayer electrostatic energy, curvature stress and assembly of gramicidin channels, Biochemistry 36 (1997) 5695–5701.
[45] L. Beney, E. Linares, E. Ferret, P. Gervais, Influence of the shape of phospholipid vesicles on the measurement of their size by photon correlation spectroscopy, Eur. Biophys. J. 27 (1998) 567–574.
[46] J. Mou, D.M. Czajkowsky, Z. Shao, Gramicidin A aggregation in supported gel state phosphatidylcholine bilayers, Biochemistry 35 (1996) 3222–3226.
[47] D. Gallez, H.M. McConnell, Coupling of size and shape equilibration in lipid monolayer domains, J. Phys. Chem. B 104 (2000) 1657–1662.
[48] P.S. Cremer, S.G. Boxer, Formation and spreading of lipid bilayers on planar glass supports, J. Phys. Chem. B 103 (1999) 2554–2559.